A Posteriori Error Estimation and Adaptive Discretization Refinement Using Adjoint Methods in CEM: A Study with a One-Dimensional Higher-Order FEM Scattering Example

Cam Key, *Student Member, IEEE*, Aaron Smull, *Student Member, IEEE*, Donald Estep, Troy Butler, and Branislav M. Notaroš, *Fellow, IEEE*

***Abstract*—This study investigates and evaluates applications of the adjoint problem and its solution in frequency-domain computational electromagnetics (CEM). The study establishes and validates adjoint-based applications including higher-order parameter sampling, a posteriori error estimate evaluation, and *p*- and *h*-refinements. These applications can improve efficiency, automation, and robustness of CEM methods. We employ a one-dimensional finite-element-method scattering solver, simplifying implementation, replicability, clarity, and intuitiveness of analysis results and conclusions, which then extend naturally to higher-dimensional solvers and more-complicated CEM problems. While demonstrated with a higher-order solver, the derived techniques apply to low-order methodology as well. This is the first demonstration of applicability of adjoint-based a posteriori error estimation techniques to adaptive discretization refinement in frequency-domain CEM with arbitrary-order basis functions. This work introduces application of dual-weighted residual error estimation and selective adaptivity based on error cancellation. The proposed targeted, adaptive mesh/model *p*- and/or *h*-refinement heuristics informed by adjoint element-wise error contribution estimates show near-monotonic reduction of quantity-of-interest error with increased number of refined elements. In general, adjoint techniques are under-utilized in CEM, and another goal of this work is to promote their future use for refinement, optimization, and uncertainty quantification.**

***Index Terms*—computational electromagnetics; finite element method; higher-order techniques, uncertainty quantification; adjoint methods; *p*-refinement; *h*-refinement; a posteriori error estimation; element-wise error contribution estimates; adaptive mesh refinement; higher-order parameter sampling; optimization.**

Manuscript received July 5, 2018, revised April 17, 2019. This work was supported by the US Air Force Research Laboratory, CREATE SENTRi, Riverside Research Institute, under contract FA8650-14-D-1725(6F1957).

Cam Key and Branislav M. Notaroš are with Department of Electrical and Computer Engineering, Colorado State University, Fort Collins, CO 80523-1373 USA. Aaron P. Smull is with the Department of Electrical and Computer Engineering at Colorado State University, Fort Collins, CO 80523-1373 USA, and the Department of Physics at the University of California, Berkeley, CA, 94720-7300, USA (e-mail: camkey@rams.colostate.edu, notaros@colostate.edu, asmull@berkeley.edu).

Donald Estep is with the Department of Statistics, Colorado State University, Fort Collins, CO, USA (e-mail: Donald.Estep@colostate.edu).

Troy Butler is with the Department of Mathematical and Statistical Sciences, University of Colorado Denver, Denver, CO, USA (email: Troy.Butler@ucdenver.edu).

I. Introduction

In the majority of computational electromagnetics (CEM) methods, numerical discretization relies on low-order techniques, for which the structure of interest is modeled by volume or surface elements that are electrically small, and the fields or currents within the elements are approximated by low-order basis functions, often resulting in large linear system size and high computational overhead. Alternatively, higher-order techniques can greatly reduce the number of unknowns for a given problem and enhance the accuracy and efficiency of the CEM analysis, utilizing higher-order basis functions, e.g., sets of linearly-independent polynomials, defined over relatively large geometrical elements [1]. This allows for much greater flexibility in adjusting the resolution of the discretization, including *h*-refinement where the element size is adjusted, *p*-refinement where the basis function order is adjusted, and *hp*-refinement which combines both approaches. However, the practical application of that flexibility still presents a significant challenge. Choosing which subset of elements to *p*- or *h*-refine to most-optimally improve solution accuracy remains an open challenge with both the higher-order methodology and low-order techniques.

Previous literature on higher-order CEM techniques has focused mainly on solver efficiency, computation times, and convergence properties with respect to *p*- or *h*-refinement in the contexts of both finite element method (FEM) and method of moments (MoM) based numerical discretization procedures, while offering some general heuristics for discretization (mesh or model) building and discretization refinement [1]-[13]. However, increasing demands of uncertainty quantification for complicated engineering simulations [14] necessitate accurate error estimation of computed results, preferably using approaches that quantify the contributions to error from various discretization choices involved in the simulation.

A practical issue with FEM and MoM CEM techniques in general is the relative inefficiency of gradient-based optimization. Many of the most effective optimization techniques rely on gradient information—in the CEM case, sensitivity of some property of the solution, the Quantity of Interest (QoI), e.g., radar cross-section (RCS), input

impedance, etc., to some parameter of the electromagnetic structure in question (scatterer shape, material permittivity, etc.). This sensitivity information is expressed as a partial derivative of the QoI with respect to the input parameter, which is obtained in the classical approach by introducing a small perturbation to the input parameter and recording the corresponding change in the output quantity. This technique requires a minimum of two complete solves—one with the nominal value and the other with the perturbed value of the parameter and is subject to issues of subtractive cancellation that necessitate accurate solves for the differences. To compound this, CEM optimization problems are often multidimensional, with several parameters forming a basis for the search space. So, the full gradient of the QoI over an n-dimensional parameter space requires n+1 full solves. For practical CEM problems, the computation time of which can often be measured in hours and sometimes days, this classical approach can be untenable.

As an optimization algorithm explores the search space, the parameters of the CEM problem being solved may vary substantially, a challenge associated with optimization applied to higher-order and low-order FEM and MoM techniques that has broader implications for both traditional (including gradient information) and gradient-free optimization techniques, like genetic algorithms and particle swarm optimization. For optimization problems with large search spaces, a sufficiently-refined mesh for all possible parameter combinations within the search bounds is often extremely fine, slowing the simulation time for each evaluation of the objective function. Rather than attempting to preconstruct a one-size-fits-all mesh, it is often advantageous to begin with a coarse discretization and refine progressively as parameter changes necessitate. This, however, potentially introduces a remeshing step between successive evaluations of the objective function (FEM or MoM solves). Each remeshing can add significant computational overhead to the optimization algorithm and raises issues regarding which elements to refine for maximum benefit and how to refine them.

We often need to improve the accuracy of an existing CEM solution to a given problem by p-, h-, or hp-refining the model adaptively. In adaptive CEM schemes, the solution is automatically refined step by step, according to an error indicator which can be derived from a posteriori error estimates, computed from the existing numerical solution at each step. Ideally, the adaption to reduce the global error in the QoI would be selective and targeted; an element would be selected for refinement based on its a posteriori error contribution estimate, with selected elements subject to a change in field or current approximation order, split into smaller elements, or both. It is therefore highly desirable to produce an automated, adaptive, targeted refinement algorithm that can not only quickly refine the discretization, but can do so near-optimally, choosing the best K elements in the mesh to p- or h-refine for the largest increase in solution accuracy for a given QoI and a given K.

Adjoint methods, employing a generalization of the notion of a Green's function, and a posteriori error estimation techniques have been widely studied in the field of applied mathematics. Influential references include application to ordinary differential equations [15] and in-depth studies concerning specific and general partial differential equations (PDEs) [16]-[20]. We direct an interested reader to [18] for an excellent summary of the methods and to [16] for a thorough study of adjoint methods as they pertain to adaptive refinement for the numerical solution of differential equations in general. These methods, although well-explored from a theoretical perspective and more frequently applied in other numerical fields like computational fluid dynamics (CFD), have not seen such widespread utilization in CEM for frequency-domain techniques, and have seen very little application toward higher-order CEM techniques. Previous work on the application of adjoint methods to CEM has most often focused on their implementation and application using time-domain methods [21]-[27]. The majority of this work has focused around sensitivity analysis, the calculation of QoI gradients with respect to various input parameters, and often the application of these gradients toward optimization, either directly through gradient-based approaches or indirectly through the construction of surrogate functions [22], [24]-[29]. Most implementations have relied on finite-difference time-domain (FDTD) approaches with various modifications. Sensitivity analysis has been applied to quantify QoI response to material discontinuities [26], optimize transmission line design [27], perform sensitivity analysis for photonic devices [25], optimize antennas [23], [29], and on similar optimization problems using frequency-domain techniques. The paper [28] notably applies adjoint sensitivity analysis to a higher-order two-dimensional triangular-element FEM solver for design optimization of planar microwave devices. The optimization approach in [28] uses adjoint information only for computation of the gradient of a QoI with respect to various parameters, but it does not apply this information to remesh or quantify numerical error.

Previous work in CEM on the quantification of numerical error has focused predominantly on adjoint-free methods quantifying error in the field solution by estimating a norm directly [30]-[33] or indirectly by convergence of this norm [34]. These methods form an a posteriori error estimate from an established norm. Our approach differs substantially by our consideration of approximate error in a quantity of interest due to the solution error, rather than a norm of a quantity approximating the solution error itself, and the use of the adjoint solution toward this goal. Use of a norm can lead to a rigorous bound to the solution error, but unfortunately, these bounds often overestimate the true error due to local and global cancellation effects. By neglecting the norm, our work exploits cancellation effects for more-accurate estimates and more precisely targeted refinement of the discretization. While examining the solution error can be useful if the application (i.e., our motivation for solving the PDE) is unknown, we are most often interested in one or few quantities derived from the field solution, e.g., radar cross section of a scatterer. In such cases, computing an approximation of the QoI error from an existing field error estimate is often less accurate than approximating the QoI in the error directly [14], [16]. Refinement based on the former, established approach, therefore tends to oversaturate the discretization, refining more elements than necessary for the given QoI when compared to the latter approach explored in this paper. Most closely related to the a posteriori error estimation in the

present work is that of Monk and Suli [35], [36], in which the adjoint is used to derive a posteriori error bounds for the far-field pattern, with the error estimate then applied to refining the discretization. However, unlike the present work, these papers produce a highly discretization-dependent error estimate specifically for the far-field pattern, limiting its applicability to first-order (linear) finite element approaches with far-field QoI. Meanwhile, the estimate given in this present paper is presented for a general QoI (with backscattered field given as an example QoI) and is broadly applicable to FEM solvers of arbitrary basis function order. This allows application to *h*-refinement, similar to [36], and rapidly-convergent *p*-refinement and *hp*-refinement. In three-dimensional cases, the error estimates defined in this paper are straightforwardly extensible to elements of arbitrary geometric shapes, while the estimate given in [35] is defined specifically for tetrahedra. Unlike [30]-[36], the present work also gives in-depth examples of the broadly applicable sensitivity information that can be attained inexpensively where the adjoint problem is solved (for instance for error estimation) and a discussion of its applications.

In this paper, we investigate useful applications of the adjoint problem and its solution toward frequency-domain CEM methods. We demonstrate how QoIs can be expressed in inner product form and show how this form can efficiently generate gradient information for a given QoI with any number of parameters using the adjoint solution. We give two useful examples of such parameters using the backscattered field amplitude as the QoI. A one-dimensional higher-order FEM scattering solver is chosen as an ideal testbed to investigate the usefulness of the proposed techniques due to its conceptual and computational simplicity, ease of implementation and replicability, and the clarity with which results from a one-dimensional model can be displayed. Namely, it is advantageous to represent much of the information obtained by adjoint methods as a scalar field over the computational domain, which facilitates displaying data in a useful and intuitive manner and enables straightforward qualitative and quantitative conclusions of the analyses. Results and observations from this model extend naturally to higher-dimensional solvers and more-complicated CEM techniques and problems. Describing how the gradient information can be used to produce a reconstruction of a QoI's response to varying parameters, we invoke the higher-order parameter sampling (HOPS) technique [37] to produce these reconstructions with applications to the example problem. We highlight how such gradient information and response reconstructions can be applied to practical CEM problems requiring many solves, for instance, RCS computation, antenna design, optimization, and Monte Carlo simulation. We introduce a posteriori error estimation techniques using the adjoint solution [38], and apply these error estimates to novel targeted *p*- and *h*-refinement schemes. To the best of our knowledge, this is the first demonstration of the applicability of both adjoint-based a posteriori error estimation and adaptive discretization refinement in frequency-domain CEM using arbitrary-order basis functions. In addition, this paper introduces to CEM the application of a dual-weighted residual (DWR) estimate to the adjoint-informed a posteriori error estimation, the selective adaptivity based on error cancellation, and *p*-refinement using the adjoint solution. The adjoint-based DWR technique for CEM proposed in this work produces an accurate, signed error estimate, which is exploited to cancel local error contributions by grouping. This results in rapid reduction in global QoI error with a high selectivity not possible using existing norm-based error estimates in CEM that seek to rigorously (or approximately) bound error in a norm.

For a useful and broadly-applicable means of evaluating the performance of different refinement approaches, we introduce a metric based on the degree of monotonicity of a given refinement to quantify its efficacy in comparison with other approaches. Using the same example scattering problem, we propose targeted, adaptive discretization (mesh or model) refinement heuristics informed by adjoint element-wise error contribution estimates. These heuristics perform exceptionally well, greatly reducing error in a QoI for only modest increases in the number of unknowns, while also near-monotonically reducing error with respect to an increasing number of refined elements. The results demonstrate the benefits that adjoint techniques offer for adaptive *p*- and *h*-refinement schemes using these heuristics. Although demonstrated with a higher-order solver, all derived and applied techniques generalize to low-order methodology, and the results in this study show the usefulness and efficiency of the proposed techniques to low-order methods with *h*-refinement only. A goal of this work is also to promote the use of adjoint approaches within future CEM techniques and implementations as a means of attaining useful refinement, optimization, and uncertainty quantification methodologies. Some preliminaries of this study are presented in a summary form in [39] and [40].

Section II describes the one-dimensional scattering test problem and briefly outlines the higher-order one-dimensional FEM implementation and its relevant components. Section III describes the theory behind the adjoint techniques demonstrated, providing specific formulae for an example QoI, gradients of this QoI with respect to two example parameters, QoI error estimation, and element-wise error contribution estimation. Section IV gives extensive and clear numerical results for adjoint methods theoretically outlined in Section III. Section IV shows reconstruction of QoI response to example parameters using the HOPS technique, element-wise error contribution estimates over the computational domain, and a comparison of illustrative targeted refinement methods based on such estimates for both *p*- and *h*-refinements. Section V then summarizes the main conclusions of the study, putting them in a broader perspective of CEM research and practice.

II. One-Dimensional Scattering Problem Solved by Higher-Order PML-Truncated FEM

We consider a simple electromagnetic scattering problem—the infinite lossy dielectric slab scatterer in a one-dimensional domain—so that the underlying physics, solutions, and numerical method parameters are straightforward to describe. We define the model domain and material subdomains for an infinite (in *y* and *z*) dielectric slab with air and a perfectly matched layer (PML) domain on either side as specified in Table I.

Table I: Model domain and material subdomains for scattering from the infinite (in *y* and *z*) lossy dielectric slab truncated by PML.

$-t_{\mathrm{PML}} < x < 0$	Left PML subdomain (t_{PML} is the selected PML thickness)
$0 < x < \lambda$	Left air subdomain (of thickness λ)
$\lambda < x < a$	Lossy dielectric slab subdomain (of thickness $a - \lambda$)
$a < x < L$	Right air subdomain (of thickness $L - a$)
$L < x < L + t_{\mathrm{PML}}$	Right PML subdomain (of thickness t_{PML})

On this domain, we use the double-curl frequency-domain wave equation [1] and the associated boundary condition,

$$\nabla\times\mu_{\mathrm{r}}^{-1}\nabla\times\mathbf{E}^{\mathrm{sc}} - k_0^2\varepsilon_{\mathrm{r}}\mathbf{E}^{\mathrm{sc}} = -\nabla\times\mu_{\mathrm{r}}^{-1}\nabla\times\mathbf{E}^{\mathrm{inc}} + k_0^2\varepsilon_{\mathrm{r}}\mathbf{E}^{\mathrm{inc}},\quad -t_{\mathrm{PML}} < x < L + t_{\mathrm{PML}} \tag{1a}$$

$$\mathbf{n}\times\mathbf{E}^{\mathrm{sc}} = 0,\quad x = -t_{\mathrm{PML}},\quad x = L + t_{\mathrm{PML}} \tag{1b}$$

where ε_{r} and μ_{r} are complex relative permittivity and permeability of the inhomogeneous medium (tensors for anisotropic materials), $\mathbf{E}^{\mathrm{inc}}$ and $\mathbf{E}^{\mathrm{sc}}$ are the incident and scattered electric field complex intensity vectors, $k_0 = \omega\sqrt{\varepsilon_0\mu_0}$ is the free-space wave number, ω is the angular frequency of the implied time-harmonic variation, and **n** is the outward unit normal on the boundary surface. Enforcing homogeneity in the *y* and *z* directions and restricting the incident field to have only a *z* component that depends only on *x*, we simplify (1) to

$$-\frac{\mathrm{d}}{\mathrm{d}x}\frac{1}{\mu_{\mathrm{r}}(x)}\frac{\mathrm{d}}{\mathrm{d}x}E_z^{\mathrm{sc}}(x) - k_0^2\varepsilon_{\mathrm{r}}(x)E_z^{\mathrm{sc}}(x) = g(x),\quad -t_{\mathrm{PML}} < x < L + t_{\mathrm{PML}} \tag{2a}$$

$$g(x) = \frac{\mathrm{d}}{\mathrm{d}x}\left(\frac{1}{\mu_{\mathrm{r}}(x)} - 1\right)\frac{\mathrm{d}}{\mathrm{d}x}E_z^{\mathrm{inc}}(x) + k_0^2(\varepsilon_{\mathrm{r}}(x) - 1)E_z^{\mathrm{inc}}(x),\quad -t_{\mathrm{PML}} < x < L + t_{\mathrm{PML}} \tag{2b}$$

$$E_z^{\mathrm{sc}}(x) = 0,\quad x = -t_{\mathrm{PML}},\quad x = L + t_{\mathrm{PML}} \tag{3}$$

With the incident field representing a *z*-polarized plane wave propagating forward along the *x*-axis and the standard PML implementation, we have

$$E_z^{\mathrm{inc}}(x) = \begin{cases} A\mathrm{e}^{-\mathrm{j}k_0 x} & 0 < x < L \\ 0 & -t_{\mathrm{PML}} < x < 0,\ L < x < L + t_{\mathrm{PML}} \end{cases} \tag{4}$$

where we choose $A = 1$ to normalize the field. The material parameter functions in the subdomains defined in Table I are given by:

$$\varepsilon_{\mathrm{r}}(x) = \begin{cases} 1 & 0 < x < \lambda \\ \varepsilon_{\mathrm{d}} & \lambda < x < a \\ 1 & a < x < L \\ 1 - \mathrm{j}\alpha_{\mathrm{PML}} & -t_{\mathrm{PML}} < x < 0,\ L < x < L + t_{\mathrm{PML}} \end{cases} \tag{5a}$$

$$\mu_{\mathrm{r}}(x) = \begin{cases} 1 & 0 < x < L \\ 1 - \mathrm{j}\alpha_{\mathrm{PML}} & -t_{\mathrm{PML}} < x < 0,\ L < x < L + t_{\mathrm{PML}} \end{cases} \tag{5b}$$

with ε_{d} denoting the equivalent complex relative permittivity of the lossy dielectric slab of relative permittivity ε_{r} and conductivity σ [41],

$$\varepsilon_{\mathrm{d}} = \varepsilon_{\mathrm{r}} - \mathrm{j}\frac{\sigma}{\omega\varepsilon_0} \tag{6}$$

The lossy dielectric slab scattering problem is solved using a higher-order PML-truncated FEM approach similar to that described in [10], [11], [42], and [43]. The domain is discretized using line segments along the *x*-axis with scalar basis functions. This geometric simplicity allows for simple *h*-refinement (e.g., an element can be split in half just by adding a new element boundary node at its midpoint).

Like their three-dimensional counterparts in [42], the basis functions used for the one-dimensional solver are defined in a domain parameterized by a single coordinate *s* which ranges from −1 to 1. The element-specific index of the chosen basis function is given by *i*, and the field expansion order for a given element is denoted *M*. Note that the higher-order approach outlined in [42] allows for arbitrary *x*-domain sizes and arbitrary, positive field expansion orders for adjacent elements. This allows adjacent elements to be *h*- and *p*-refined to differing degrees entirely independently of each other. The *i*th basis function for an element is given in the *s* domain as:

$$u_i(s) = \begin{cases} 0.5(1 + (-1)^i s) & i = 0,1 \\ 0.5(1 - s)(1 + s)^{i-1} & 2 \le i \le M \end{cases} \tag{7}$$

The first and second basis functions maintain field continuity between adjacent elements, while the higher-order basis functions allow for additional *p*-refinement. Note that functions in (7) are just one simple choice of higher-order scalar bases on the *s*-parametric domain, and alternative hierarchical polynomial basis functions with improved orthogonality and conditioning properties could also be chosen. For example, a one-dimensional variant of those used in the higher-order FEM-PML method [43] may be easily implemented.

III. The Adjoint Solution and its Applications

A. The Adjoint Problem and the Quantity of Interest

The notion of an adjoint problem generalizes the method of Green's functions [38], [44], [45]. To define the adjoint operator for a given problem, we must cast the problem in linear operator form. For the lossy dielectric slab scattering problem, we consider the Dirichlet boundary value problem given in (2)-(3). The differential equation in (2a) can be expressed in linear operator form as

$$L\mathbf{E}_z^{\mathrm{sc}} = \mathbf{g} \tag{8}$$

L represents the "forward" operator the forward solution (the scattered electric field), designated $\mathbf{E}_z^{\mathrm{sc}}$. The adjoint operator of *L* is the operator L^{adj} that satisfies the Lagrange identity [38],

$$\left\langle \mathbf{E}^{\mathrm{adj}}, L\mathbf{E}_z^{\mathrm{sc}} \right\rangle = \left\langle L^{\mathrm{adj}}\mathbf{E}^{\mathrm{adj}}, \mathbf{E}_z^{\mathrm{sc}} \right\rangle \tag{9}$$

with angle brackets denoting the L^2 inner product on functions. The data for the adjoint problem is, in this case, a QoI determined by a linear functional on the forward solution. In inner product form, the QoI is given as

$$\mathrm{QoI} = q[\mathbf{E}_z^{\mathrm{sc}}] = \left\langle \mathbf{E}_z^{\mathrm{sc}}, \mathbf{p} \right\rangle \tag{10}$$

where $\mathbf{p}$ is a function that determines an instrumental or measurement characteristic. For instance, the QoI could be chosen as the field value at a given point in the domain by defining $\mathbf{p}$ as a Dirac delta function at that point, in which case the adjoint solution is the Green's function [45]. The sampling property of the Dirac delta function when the inner product is applied then evaluates the field at one point. For a given measurement characteristic, the adjoint problem is

$$L^{\mathrm{adj}}\mathbf{E}^{\mathrm{adj}} = \mathbf{p} \tag{11}$$

Note that, in a physical interpretation of (11), the measurement characteristic defining some QoI on the forward solution becomes the excitation of the adjoint problem. As $\mathbf{p}$ defines a unique QoI, (11) implies that the adjoint equation must be re-solved with a new right-hand-side for each new QoI, analogous to re-solving a forward problem with new incident fields.

In our study, we choose a QoI that yields the magnitude of the reflected field from the lossy dielectric slab subject to some incident field. We express the solution in the air-filled region $0 < x < \lambda$ as

$$E_z^{\mathrm{sc}}(x) = E_{\mathrm{i},z}\mathrm{e}^{-\mathrm{j}k_0 x} + E_{\mathrm{r},z}\mathrm{e}^{\mathrm{j}k_0 x},\ 0 < x < \lambda \tag{12}$$

where $E_{\mathrm{i},z}$ and $E_{\mathrm{r},z}$ are (complex-valued) numbers characterizing the forward and backward traveling electromagnetic fields, respectively. Since $A = 1$ in (4) and the zero-phase point of the reflected field is $x = 0$, $E_{\mathrm{r},z}$ is equal to the complex reflection coefficient. We express the amplitude of the reflected field as a QoI in inner product form (10) as

$$\begin{aligned} q[\mathbf{E}_z^{\mathrm{sc}}] &= \frac{k_0}{2\pi}\int_0^{2\pi/k_0} \mathrm{e}^{-\mathrm{j}k_0 x}\mathbf{E}_z^{\mathrm{sc}}\,\mathrm{d}x \\ &= \left\langle \mathbf{E}_z^{\mathrm{sc}}, \frac{k_0}{2\pi}\mathrm{e}^{\mathrm{j}k_0 x}\left[H(x) - H(x - \frac{2\pi}{k_0})\right] \right\rangle = \left\langle \mathbf{E}_z^{\mathrm{sc}}, \mathbf{p} \right\rangle \end{aligned} \tag{13}$$

where $H(x)$ is the unit step (Heaviside) function and $\mathbf{p}$ denotes the defined measurement characteristic. The behavior of this QoI can be evaluated from (13) on a function of the form (12) yielding

$$q[E_{\mathrm{i},z}\mathrm{e}^{-\mathrm{j}k_0 x} + E_{\mathrm{r},z}\mathrm{e}^{\mathrm{j}k_0 x}] = E_{\mathrm{r},z} \tag{14}$$

Note that in (14), it is assumed that the surface of the dielectric slab is outside the limits of integration. The idea behind this type of functional evaluation is easily extended to a higher-dimensional scattering problem—different components of the spatial Fourier transform of a scattered electromagnetic wave along a closed surface in free space effectively gives the scattered electromagnetic field in different far-field directions.

To derive the adjoint operator for (2a), we apply the Lagrange identity in (9), where the left-hand side of (9) may be expressed as

$$\begin{aligned} &\int_{-t_{\mathrm{PML}}}^{L+t_{\mathrm{PML}}} E^{\mathrm{adj}*}(x)\left(-\frac{\mathrm{d}}{\mathrm{d}x}\frac{1}{\mu_{\mathrm{r}}(x)}\frac{\mathrm{d}}{\mathrm{d}x}E_z^{\mathrm{sc}}(x)\right)\mathrm{d}x - \\ &\int_{-t_{\mathrm{PML}}}^{L+t_{\mathrm{PML}}} E^{\mathrm{adj}*}(x)\left(k_0^2\varepsilon_{\mathrm{r}}(x)E_z^{\mathrm{sc}}(x)\right)\mathrm{d}x \end{aligned} \tag{15}$$

with E^{adj} denoting the unknown adjoint solution. Integrating the first term in (15) by parts, it becomes

$$\begin{aligned} &-E^{\mathrm{adj}*}(x)\frac{1}{\mu_{\mathrm{r}}(x)}\frac{\mathrm{d}}{\mathrm{d}x}E_z^{\mathrm{sc}}(x)\Big|_{-t_{\mathrm{PML}}}^{L+t_{\mathrm{PML}}} + \\ &\int_{-t_{\mathrm{PML}}}^{L+t_{\mathrm{PML}}} \frac{1}{\mu_{\mathrm{r}}(x)}\frac{\mathrm{d}}{\mathrm{d}x}E_z^{\mathrm{sc}}(x)\frac{\mathrm{d}}{\mathrm{d}x}E^{\mathrm{adj}*}(x)\mathrm{d}x \end{aligned} \tag{16}$$

Then integration of the second term of (16) by parts results in

$$\begin{aligned} &E_z^{\mathrm{sc}}(x)\frac{1}{\mu_{\mathrm{r}}(x)}\frac{\mathrm{d}}{\mathrm{d}x}E^{\mathrm{adj}*}(x)\Big|_{-t_{\mathrm{PML}}}^{L+t_{\mathrm{PML}}} - \\ &\int_{-t_{\mathrm{PML}}}^{L+t_{\mathrm{PML}}} E_z^{\mathrm{sc}}(x)\frac{\mathrm{d}}{\mathrm{d}x}\frac{1}{\mu_{\mathrm{r}}(x)}\frac{\mathrm{d}}{\mathrm{d}x}E^{\mathrm{adj}*}(x)\mathrm{d}x \end{aligned} \tag{17}$$

Applying the forward boundary conditions from (3), we cancel the first term of (17). By similarly cancelling the first term in (16), we enforce the adjoint boundary conditions,

$$\begin{aligned} E^{\mathrm{adj}}(L + t_{\mathrm{PML}}) &= 0 \\ E^{\mathrm{adj}}(-t_{\mathrm{PML}}) &= 0 \end{aligned} \tag{18}$$

The FEM approach studied in this paper utilizes in general a PML terminated in a perfect electric conductor (PEC) to truncate the computational domain. As such, this treatment of the first term in (16) and (17) is universally applicable for this method and is analogously true in two and three dimensions. We next rewrite (15) by rearranging its second term and applying the results of integration by parts, yielding

$$\begin{aligned} &-\int_{-t_{\mathrm{PML}}}^{L+t_{\mathrm{PML}}} E_z^{\mathrm{sc}}(x)\frac{\mathrm{d}}{\mathrm{d}x}\frac{1}{\mu_{\mathrm{r}}(x)}\frac{\mathrm{d}}{\mathrm{d}x}E^{\mathrm{adj}*}(x)dx - \\ &\int_{-t_{\mathrm{PML}}}^{L+t_{\mathrm{PML}}} E_z^{\mathrm{sc}}(x)k_0^2\varepsilon_{\mathrm{r}}(x)E^{\mathrm{adj}*}(x)dx \end{aligned} \tag{19}$$

from which we recover the form of the adjoint operator on the right-hand side of (9) by taking the complex conjugate,

$$L^{adj}E^{\mathrm{adj}} = -\frac{\mathrm{d}}{\mathrm{d}x}\frac{1}{\mu_{\mathrm{r}}^{*}(x)}\frac{\mathrm{d}}{\mathrm{d}x}E^{\mathrm{adj}}(x) - k_0^2\varepsilon_{\mathrm{r}}^{*}(x)E^{\mathrm{adj}}(x) = p(x) \tag{20}$$

Note the similarity of the adjoint equation (20) to the forward equation (2a). We see that the one-dimensional analogue of the double-curl wave equation (1a) is nearly self-adjoint, its adjoint being described entirely by complex conjugation of the material parameters.

B. A Posteriori Error Estimation and p-/h-Refinement

Accurate estimation of error in computational simulation results is a key component in uncertainty quantification [14]. Additionally, adaptive *p*- and *h*-refinement schemes require indicators of the error in a QoI on which the adaption is done, namely, new field/current approximation orders and/or new element sizes are assigned in the new, refined model. Furthermore, in CEM problems requiring many computational simulations, it is useful to have an estimate of whether accuracy of a forward solution for a given parameter set and discretization is sufficient for the desired tolerance, or if refinement is needed for subsequent solves. Such problems, including optimization, antenna design, and radar cross-section determination, are common in CEM. An adjoint-based a posteriori error estimate can address each of these needs.

Due to the Galerkin orthogonality property [45], computing this error estimate essentially involves evaluating a numerical approximation to derivatives of the adjoint solution, and therefore requires that the adjoint problem be solved on a discretization different than that used for the forward solution, for instance, using either finer geometric elements or higher-order basis functions. In general, the adjoint discretization need not present more unknowns than the forward discretization, but for more-accurate estimates it is desirable to compute the adjoint solution using a finer discretization. The use of hierarchical basis functions in this work makes the calculation of many of the required degrees of freedom simpler.

We express the numerical solution of the forward problem on a given mesh as

$$\mathbf{E}_z^{\mathrm{sc}} \approx \tilde{\mathbf{E}}_z^{\mathrm{sc}} = \sum_{u_i \in \mathbf{V}_{\mathrm{b}}} \alpha_i u_i(x), \tag{21}$$

where $\mathbf{V}_{\mathrm{b}}$ is the space of basis functions for the forward solution. Additionally, we express the numerical solution to the adjoint equation by

$$\mathbf{E}^{\mathrm{adj}} \approx \tilde{\mathbf{E}}^{\mathrm{adj}} = \sum_{u_i \in \mathbf{V}_{\mathrm{b}'}} \beta_i u_i(x), \tag{22}$$

with $\mathbf{V}_{\mathrm{b}'}$ designating the space of basis functions for the adjoint problem, where the *M* in (7) for each element has been increased by 1 from $\mathbf{V}_{\mathrm{b}}$. Also, we let $\pi_{\mathrm{h}}\tilde{\mathbf{E}}^{\mathrm{adj}}$ denote a projection or interpolant of the adjoint solution into the discrete space $\mathbf{V}_{\mathrm{b}}$ in which we numerically solve the forward problem. In this work, $\pi_{\mathrm{h}}\tilde{\mathbf{E}}^{\mathrm{adj}}$ is defined by a least squares approximation of $\tilde{\mathbf{E}}^{\mathrm{adj}}$ in the $\mathbf{V}_{\mathrm{b}}$ subspace of $\mathbf{V}_{\mathrm{b}'}$. Following the arguments expressing the QoI in terms of the adjoint solution above, the a posteriori estimate on the error in the QoI is

$$\begin{aligned}\left\langle \mathbf{E}_z^{\mathrm{sc}} - \tilde{\mathbf{E}}_z^{\mathrm{sc}}, \mathbf{p} \right\rangle \approx & \left\langle g(x), \tilde{\mathbf{E}}^{\mathrm{adj}} - \pi_{\mathrm{h}}\tilde{\mathbf{E}}^{\mathrm{adj}} \right\rangle \\ & - \left\langle \frac{1}{\mu_{\mathrm{r}}(x)}\frac{\mathrm{d}}{\mathrm{d}x}\tilde{\mathbf{E}}_z^{\mathrm{sc}}, \frac{\mathrm{d}}{\mathrm{d}x}\tilde{\mathbf{E}}^{\mathrm{adj}} - \frac{\mathrm{d}}{\mathrm{d}x}\pi_{\mathrm{h}}\tilde{\mathbf{E}}^{\mathrm{adj}} \right\rangle \\ & + k_0^2 \left\langle \varepsilon_{\mathrm{r}}(x)\tilde{\mathbf{E}}_z^{\mathrm{sc}}, \tilde{\mathbf{E}}^{\mathrm{adj}} - \pi_{\mathrm{h}}\tilde{\mathbf{E}}^{\mathrm{adj}} \right\rangle\end{aligned} \tag{23}$$

Essentially, (23) represents the inner product (in weak form) of the residual of $\tilde{\mathbf{E}}_z^{\mathrm{sc}}$ and a weight determined by the adjoint solution $\tilde{\mathbf{E}}^{\mathrm{adj}}$, so it is also called a dual-weighted residual (DWR) estimate. The residual quantifies how well the numerical solution solves the differential equation while the adjoint weight quantifies how the local residual affects the global error [14].

As the adjoint-based a posteriori error estimate requires an additional numerical solve on a finer discretization, it may seem counterintuitive to spend this on an adjoint solve. We recall Richardson extrapolation suggests the classical approach to obtain an error estimate on the accuracy of a forward solution on a given discretization, which is obtained by subtracting the forward solution from a more accurate forward solution obtained from a refined discretization. Because the classic estimate is on the error of the solution rather than a QoI, the level of refinement needed for reliably accurate estimates using the classical approach is generally higher than needed to compute an accurate a posteriori error estimate [14]. Moreover, the classical approach does not yield an estimate on a QoI that distinguishes residuals determined by local discretization choices and the effects of stability as determined by the adjoint solution, hence the classical estimate is less useful for adaptive discretization [14]. Finally, once obtained, the adjoint solution can be used for other purposes, e.g., optimization and sensitivity analysis.

The standard FEM implementation computes integrals through the domain element-by-element; the inner product integrals in (23) are evaluated in a similar manner, with integrals first computed over each element separately and then summed to obtain the final error estimate. The information at the intermediate step before summation is immensely useful toward remeshing and determining which locations in the mesh are most in need of refinement. This information is referred to as the element-wise error contribution estimate and can be represented as a vector of error contribution estimates from each element

$$\mathbf{e} = (e_1, e_2, ..., e_N) \tag{24}$$

where e_i denotes the error contribution of the *i*th element and *N* is the total number of elements. The sum of (24) then gives the total QoI error estimate.

C. Obtaining and Utilizing Gradient Information from the Adjoint Solution

A classical first-order finite difference approach to compute the gradient of a QoI with respect to P independent parameters requires a minimum P+1 solves of the forward problem. Using adjoint methods, the same gradient information is obtained using a single adjoint solve over a finer discretization as expressed in (22), requiring only an expression of the partial derivative of the operator with respect to each parameter as shown below. From [38], we use a Taylor expansion of the QoI, represented here in inner product form as in (10), at an arbitrary parameter value, r, in terms of a known value of that QoI for a nominal parameter value, r_0,

$$\left\langle \mathbf{E}_z^{\mathrm{sc}}, \mathbf{p} \right\rangle = \left\langle \mathbf{E}_{z,0}^{\mathrm{sc}}, \mathbf{p} \right\rangle + \left\langle LD_r \mathbf{E}_{z,0}^{\mathrm{sc}}(r - r_0), \mathbf{E}^{\mathrm{adj}} \right\rangle + \left\langle \mathbf{R}, \mathbf{E}^{\mathrm{adj}} \right\rangle \quad (25)$$

where $\mathbf{E}_{z,0}^{\mathrm{sc}}$ represents the forward solution at r_0, D_r denotes the Frechet derivative operator, in this case with respect to r, and $\mathbf{R}$ is a higher-order remainder term.

Neglecting the remainder term, we obtain a linear approximation for the QoI around the nominal parameter value using the higher-order parameter sampling (HOPS) method [37],

$$\left\langle \mathbf{E}_z^{\mathrm{sc}}, \mathbf{p} \right\rangle \approx \left\langle \mathbf{E}_{z,0}^{\mathrm{sc}}, \mathbf{p} \right\rangle + \left\langle LD_r \mathbf{E}_{z,0}^{\mathrm{sc}}(r - r_0), \mathbf{E}^{\mathrm{adj}} \right\rangle \quad (26)$$

with the partial derivative of the QoI with respect to the chosen parameter near the nominal parameter value given by

$$\frac{\partial q}{\partial r}(r_0) = \left\langle LD_r \mathbf{E}_{z,0}^{\mathrm{sc}}, \mathbf{E}^{\mathrm{adj}} \right\rangle \quad (27)$$

The gradient of a QoI with respect to multiple parameters, each around a nominal value, can then be formed by a vector of partial derivatives of form (27), requiring only the evaluation of inner products with an adjoint solution, rather than numerous additional perturbed solutions of the forward problem.

To briefly demonstrate where (27) comes from and how the $LD_r\mathbf{E}_0^{\mathrm{sc}}$ term may be evaluated, we begin by noting

$$D_r q = D_r \left\langle \mathbf{E}_z^{\mathrm{sc}}, \mathbf{p} \right\rangle = \left\langle D_r \mathbf{E}_z^{\mathrm{sc}}, \mathbf{p} \right\rangle \quad (28)$$

Applying (9) and (11), we then get

$$D_r q = \left\langle LD_r \mathbf{E}_z^{\mathrm{sc}}, \mathbf{E}^{\mathrm{adj}} \right\rangle \quad (29)$$

Now applying the Frechet derivative operator to both sides of (8), we write

$$\begin{aligned} &D_r[L\mathbf{E}_z^{\mathrm{sc}} = \mathbf{g}] = [D_r L\mathbf{E}_z^{\mathrm{sc}} + LD_r \mathbf{E}_z^{\mathrm{sc}} = D_r \mathbf{g}] \\ &LD_r \mathbf{E}_z^{\mathrm{sc}} = D_r \mathbf{g} - D_r L\mathbf{E}_z^{\mathrm{sc}} \end{aligned} \quad (30)$$

IV. Numerical Results and Discussion

A. HOPS for the Lossy Dielectric Slab Scatterer

We first present results for HOPS described in Section III.C applied to the lossy dielectric slab scattering problem described in Section II with the reflected field amplitude QoI described in Section III.A. Implementing HOPS for two parameters, the imaginary part of the slab relative permittivity and the left slab-air interface location, we show the efficacy of this technique in obtaining derivative information and approximate reconstructions of QoI response to changing parameters from only a few sample points.

Separating the slab complex relative permittivity into real and imaginary parts,

$$\varepsilon_{\mathrm{r}}(x) = \alpha + \mathrm{j}\beta, \quad \lambda < x < a \quad (31)$$

we choose β as the HOPS parameter with nominal value β_0. The linear approximation of the QoI around β_0 can then be expressed in the form of (26) as

$$\begin{aligned} &q(\beta) \approx q(\beta_0) + \\ &\left\langle [-\mathrm{D}_\beta(-k_0^2 \varepsilon_{\mathrm{r}}(x)\mathbf{E}_{z,0}^{\mathrm{sc}}) + \mathrm{D}_\beta(k_0^2(\varepsilon_{\mathrm{r}}(x) - 1)\mathbf{E}_z^{\mathrm{inc}})], \mathbf{E}_0^{\mathrm{adj}} \right\rangle (\beta - \beta_0) \end{aligned} \quad (32)$$

which, writing the inner products in integral form, is given by

$$q(\beta) \approx q(\beta_0) + (\beta - \beta_0)\mathrm{j}k_0^2 \int_\lambda^a (E_{z,0}^{\mathrm{sc}}(x) + E_z^{\mathrm{inc}}(x)) E_0^{\mathrm{adj}*}(x) dx \quad (33)$$

Note that all integrals over elements within the slab required for evaluation of (33) are calculated during assembly of the stiffness matrix for the FEM, provided each element in the integration domain has a homogeneous permittivity value. The HOPS technique is applied to a set of 5 nominal parameter values to reconstruct the response of the QoI to β. Results generated using first-order forward solves and second-order adjoint solves with h-uniform elements are overlaid in Fig. 1 with the QoI response over the same parameter range obtained by analytical solution of (2)-(3). Each of the five lines obtained by (33) at the five sample points is truncated at intersections with its left and right neighbors to produce a piecewise-linear reconstruction of the QoI response.

The five-point HOPS results in Fig. 1 agree very closely with the analytical solution, both in the real component and imaginary component, despite a large parameter domain and low number of sample points. A piece-wise linear approximation of a QoI response in this form has many useful applications. For instance, such an approximation could be used as an inexpensive surrogate function for optimization, requiring fewer expensive direct evaluations of the QoI response by forward solves. The approach in (33) can be easily extended to variations in other material parameters and higher-dimensional problems, requiring only an expression for $LD_r\mathbf{E}_0^{\mathrm{sc}}$ from the chosen problem.

It is often of great interest in practical CEM problems to determine effects of the location of a material interface on some QoI, for instance the response of the RCS in a given direction to the shape of a scatterer. We give a one-

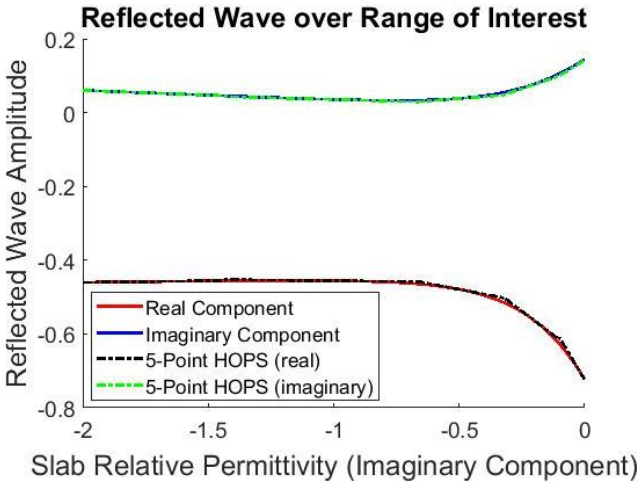

Fig. 1. Higher-order parameter sampling using five sample points to produce a linear reconstruction of the response of the reflected field amplitude to the imaginary component of the slab relative permittivity. Results are generated using first-order forward solves and second-order adjoint solves. The domain length is L = 4 m, the slab left boundary location is λ = 1 m, the frequency is f = 600 MHz, and the real part of the slab relative permittivity is α = 7. Elements are h-uniform with size 0.02 m. Samples were taken at β = [−2.0, −1.0, −0.5, −.025, 0].

dimensional analogue of this problem here, choosing the analogous QoI from (13) and approximating its response to changes in the left slab interface location λ. The permittivity function in the subdomain $0 < x < L$ can be represented in terms of unit step functions as

$$\varepsilon_r(x) = 1 + (\varepsilon_d - 1)H(x - \lambda_0) - (\varepsilon_d - 1)H(x - a) \tag{34}$$

We may approximatively express $q(\lambda)$, again using the HOPS method from (26), as

$$q(\lambda) \approx q(\lambda_0) + k_0^2 \left\langle [-\mathrm{D}_\lambda(\varepsilon_r(x)\mathbf{E}_{z,0}^{sc}) + \mathrm{D}_\lambda((\varepsilon_r(x) - 1)\mathbf{E}_z^{inc})], \mathbf{E}_0^{adj} \right\rangle (\lambda - \lambda_0) \tag{35}$$

which requires the calculation of the derivative of the permittivity function (5a) with respect to λ for direct implementation. The Frechet derivative of the permittivity function can be written in terms of the Dirac delta function as

$$\mathrm{D}_\lambda \varepsilon_r(x) = -(\varepsilon_d - 1)\delta(x - \lambda_0) \tag{36}$$

which, after evaluating the inner product using the sampling property of the Dirac delta, gives a form of (35) that can be evaluated directly:

$$q(\lambda) \approx q(\lambda_0) - k_0^2 [E_0^{adj*}(x = \lambda_0)(\varepsilon_d - 1)(E_{z,0}^{sc}(x = \lambda_0) + E_z^{inc}(x = \lambda_0))](\lambda - \lambda_0) \tag{37}$$

Note that here we have assumed a piecewise constant permittivity function (34). Were the permittivity function instead smooth and continuous, evaluating the corresponding analogue of (35) becomes simpler, requiring no use of the sampling property of the Dirac delta as in (37). In fact, we only require that a function describing the material renders both sides of (8) Fréchet differentiable with respect to the chosen parameter.

Similar to Fig. 1, Fig. 2 shows results of a five-sample HOPS reconstruction of the QoI response, this time with respect to the x-coordinate of the left slab face. Results are again generated using first-order forward solves, second-order adjoint solves, and h-uniform elements. We again see excellent agreement between the HOPS result and the analytical QoI response over the parameter domain.

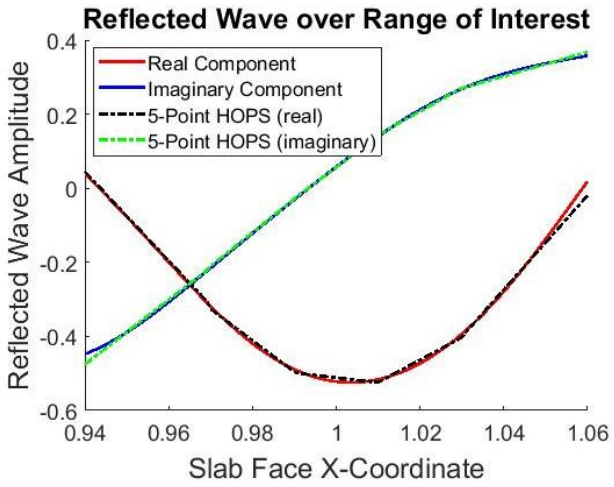

Fig. 2. Higher-order parameter sampling using five sample points to produce a linear reconstruction of the response of the reflected field amplitude to the location of the left slab face, using first-order forward solves and second-order adjoint solves, with L = 4 m, λ = 1 m, f = 600 MHz, slab relative permittivity ε_r = 7 − j1.8, and h-uniform elements of size 0.02 m. Samples were taken at λ_0 = [0.96, 0.98, 1.0, 1.02, 1.04].

B. Element-Wise Error Contributions

We next show the application of the adjoint method to obtain **e**, the element-wise error contribution estimate, for a given problem. Maintaining most parameter values from solves in Section IV.A and coarsening the element size to 0.05 m, we compute **e** through a partial (un-summed) evaluation of (23) as described in Section III.B. Fig. 3 shows the real and imaginary components of **e** plotted throughout the different material subdomains, with e_i for the ith element plotted at the x-coordinate of the element's midpoint.

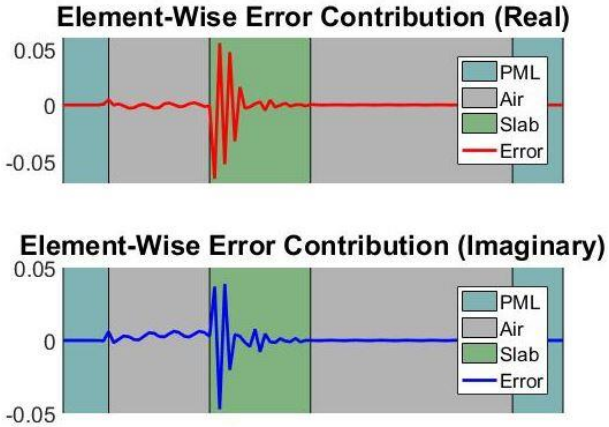

Fig. 3. Real and imaginary element-wise error contribution estimates over the computational domain. Results are generated using first-order forward solves and second-order adjoint solves, with L = 4 m, λ = 1 m, f = 600 MHz, ε_r = 7 − j1.8, and h-uniform elements of size 0.05 m.

We note several crucial things from the element-wise error contribution in Fig. 3. Most importantly, the real and imaginary error contributions are oscillatory, varying from positive to negative values through the domain. As the total error estimate is obtained by the sum of these individual error contribution estimates, we can conclude that there is a high degree of cancelation between error contributions throughout the domain. Clearly this cancelation is not complete, or the error estimate given in (23) would be zero. An interesting question then becomes where in the computational domain this lack of cancelation occurs—which elements are contributing the most to the total error estimate. This is a deceptively ill-posed problem, however, see [45]. We cannot directly assign the bulk of the residual error to any one set of elements. To do so suggests some necessary ordering to **e**.

It is difficult if not impossible to apply a universally-applicable and consistent method to identify which elements contribute the most to the total error estimate that relies on the ordering of elements in the spatial domain or the order in which error contributions are summed [45]. No ordering actually exists for the summation of **e**—the error contribution of a given element can be said to cancel with that of any other element or combination of elements, no matter how distant the elements are in the computational domain. To accurately apply this element-wise error contribution estimate toward targeted, adaptive mesh or model refinement, we must define a means by which to identify a "bad" element that relies on no such ordering. We describe such heuristics in the following section.

C. Targeted h- and p-Refinement Using Element-Wise Error Contribution Information

We show in this section the application of two un-ordered refinement heuristics and their applications to *h*- and *p*-refinement on a variety of evaluations of error in the QoI for a three-dimensional parameter space consisting of λ, α, and β. The different locations in this search space at which the QoI error estimate is evaluated are given in Table II.

Table II: Parameter space locations at which QoI error estimate is evaluated for refinement of the results in Section IV.C.

Plot Identifier	α	β	λ (m)
Case A	7	−1.8	1
Case B	7	−1.8	1.2
Case C	7	−1.8	0.8
Case D	7	−4	1
Case E	7	−4	1.2
Case F	7	−4	0.8
Case G	3	−1.8	1
Case H	3	−1.8	1.2
Case I	3	−1.8	0.8
Case J	3	−4	1
Case K	3	−4	1.2
Case L	3	−4	0.8

A refinement heuristic can be stated as one by which elements in the domain are ranked according to the expected error reduction incurred by their refinement. As described in Section IV.B, defining such a heuristic is difficult due to error cancellation effects between elements. Therefore, a successful refinement heuristic must in some way take into account the aggregate effects of error cancellation, rather than applying a ranking methodology to each element dependent only on the error contribution of that element. Additionally, the element-wise error contribution for each element does not vary exclusively with its own size or basis function order, but is instead dependent on the discretization fineness for all elements. That is to say if we have a positive total error estimate, we cannot simply refine a few of the elements with the largest positive error contributions and hope to sway the sum toward zero. This is in practice a very poor approach and will typically result in higher total error despite refinement in the mesh.

Examination of each refinement approach in this section is performed by evaluating the relative error of the QoI calculated by a forward solve on a mesh with K refined elements at each of the locations in the parameter space defined in Table II with respect to the analytical QoI at those parameter space locations. A base mesh ($K = 0$) is used for all test cases that contained 100 first-order elements of size 0.05 m. K is then varied from 0 to 100 for each simulation, using the heuristic to select a constant dK elements to refine at each subsequent refinement. *p*-refinement of an element consisted of increasing M for that element by 1, while *h*-refinement entailed splitting the element into two elements of size 0.025 m. Relative error calculated in this manner is here referred to simply as error. Adjoint solutions are calculated on meshes of one order higher than the forward solution for each location in the parameter space to obtain an error estimate for each location and K. These error estimates are added back onto the QoI to produce a corrected QoI, and the relative error of this corrected QoI which with respect to the analytical QoI is referred to as the corrected error. All relative error values are given as percentages for clarity. A vector of relative error values, formed separately for uncorrected and corrected results, is recorded for each test case. The entries of these vectors correspond to the relative errors for each K tested. To show general trends, these vectors are averaged for a given heuristic trial, giving for each a vector of average relative errors, **k**, over the range of K for both uncorrected and corrected errors.

To quantify the efficacy of various refinement heuristics, we define a so-called improvement metric as

$$I(\mathbf{k}) = \frac{\sum \text{sign}(\text{diff}(\mathbf{k}))}{\text{length}(\mathbf{k})} \tag{38}$$

where **k** represents either the uncorrected or corrected error, length(**k**) is the length of the vector **k**, and diff(**k**) returns a vector of length one lower than **k** containing the differences in value between adjacent entries of **k**. A lower value of this metric implies better performance with −1 or 1 representing a heuristic that always decreases or increases, respectively, the error with increasing number of refined elements. An I value of zero represents a heuristic that has an equal chance to increase or decrease error with additional refined elements.

The first refinement heuristic explored is referred to as the magnitude refinement heuristic. This heuristic simply ranks elements by the absolute value of their error contribution estimate, such that elements with higher error contribution estimate magnitude rank higher. Note that this heuristic does not directly satisfy our earlier desire for a heuristic that

considers aggregate error cancellation effects for refinement rather than applying a ranking methodology to each element dependent only on the error contribution of that element. Respective results for uncorrected and corrected relative errors and two different dK values for the magnitude refinement heuristic applied to p-refinement are shown in Fig. 4. Fig. 5 shows corresponding results for the magnitude refinement heuristic applied to h-refinement.

We see from Fig. 4 that the magnitude refinement heuristic informed by adjoint information reduces the QoI relative error from ~30% to <1% by K = 30 when applied to p-refinement. We also see that the corrected QoI obtained by adding the error estimate from (23) obtained by the adjoint solve to the forward QoI is vastly more accurate, with an initial relative error of ~0.42% which is reduced below 0.01% by K = 30. For K = 30, we have therefore reduced the initial error in the QoI by over three orders of magnitude with just four solves—two forward and two adjoint. Note also that all refinement performed here is entirely automated, requiring no input from the user other than a desired K, and furthermore that the technique used is not dependent on the dimension of the problem, variety of element, or volume vs. surface nature of the discretization. This demonstrates the usefulness of adjoint-assisted targeted, adaptive refinement for difficult-to-refine higher-order techniques based on the FEM and/or MoM where efficient automated discretization refinement presents a challenge.

As is inherent to the scaling of FEM and MoM error with h-refinement vs. p-refinement, we see that convergence is more-gradual in Fig. 5 for the magnitude refinement heuristic applied instead to h-refinement. We still observe desirable reduction in error, however, with the relative error decreasing from ~30% to ~10% and ~0.4% to <0.1% for K = 60. Note that this does not seek to discount the usefulness of h-refinement as a technique—a mesh (model) insufficient to describe a given problem certainly requires both h- and p-refinements to obtain a useful solution efficiently—but rather seeks to point out the power of adjoint-informed p-refinement on meshes already h-fine enough to describe the problem of interest.

The second refinement heuristic explored is more complicated and will be referred to as the greedy refinement heuristic. The greedy refinement heuristic is an approximate approach to a more-desirable but computationally-untenable approach here referred to as minimum sum grouping. Instead of seeking the K elements that should be refined, minimum sum grouping seeks a solution to the problem of which elements should not be refined. In concrete terms, it computes the subset, **e**', of entries in **e** of length length(**e**) − K the absolute value of the sum of which is the smallest possible for a given **e** and K. The K elements selected for refinement by this method are then the elements associated with the remaining K entries in **e** that are not in **e**'.

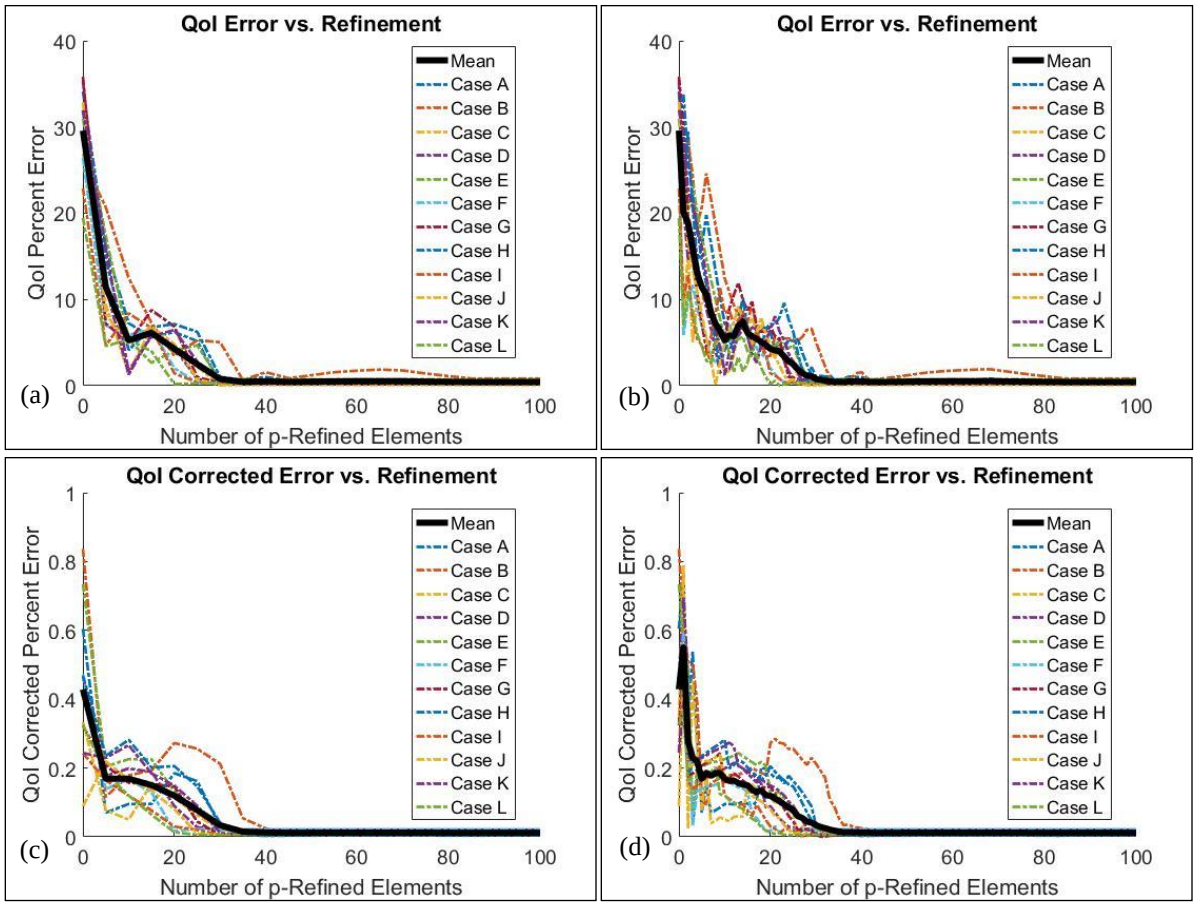

Fig. 4. Relative errors of the QoI calculated at each of the locations in the parameter space defined in Table II with respect to the analytical QoI for the magnitude refinement method implemented with p-refinement vs. the number of refined elements: (a) uncorrected error for dK = 5, (b) uncorrected error for dK = 1, (c) corrected error for dK = 5, and (d) corrected error for dK = 1.

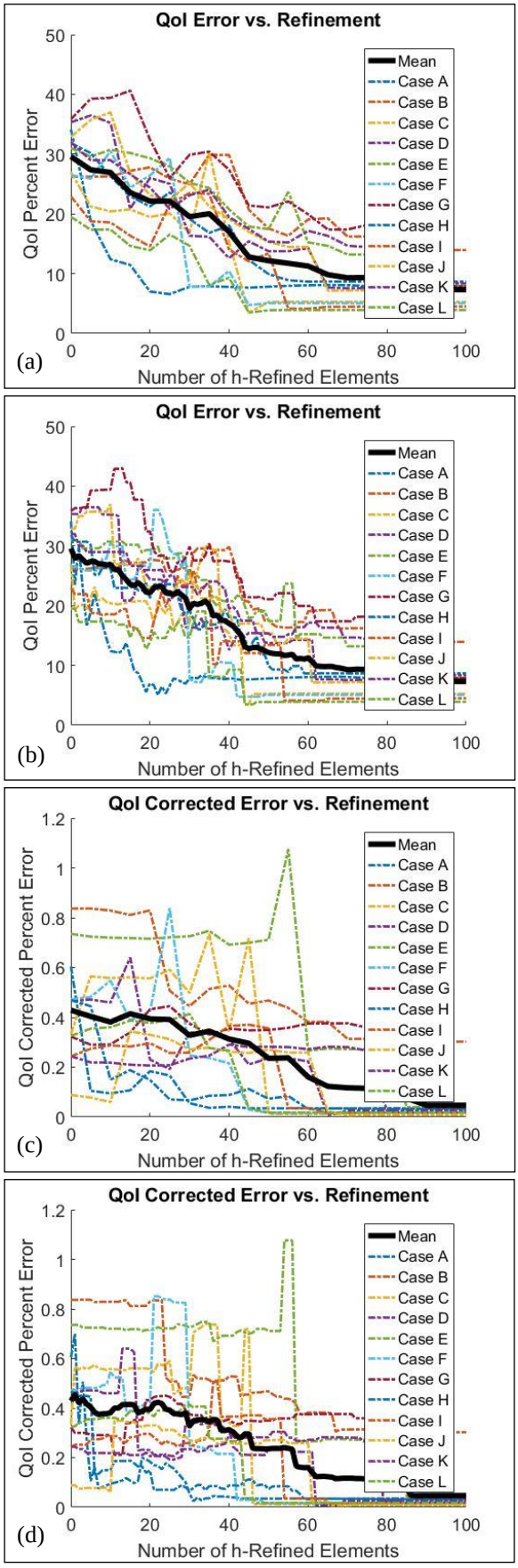

Fig. 5. The same as in Fig. 4 but for the magnitude refinement method implemented with *h*-refinement.

The subset **e**' is in practice not tenable to compute, as it requires evaluating the absolute value of the sum of all possible combinations of entries in **e** of length length(**e**) − *K*. The computational complexity of this problem scales factorially, making the application of minimum sum grouping to problems of even moderate element count computationally infeasible. Hence, we use a "greedy" refinement heuristic that offers a greedy approximate solution to the minimum sum grouping approach. We begin by computing a length(**e**) by length(**e**) matrix **S** from **e** with entries of the form

$$s_{ij} = \mathrm{abs}(e_i + e_j) \tag{39}$$

neglecting the diagonal entries ($j = i$), and we find the minimum s_{ij}, appending the corresponding e_i and e_j to an ordered list. We then select the second smallest s_{ij} in **S** that does not include any of the particular **e** entries used previously, appending its corresponding e_i and e_j to the end of the same ordered list. This is repeated until all entries of **e** have been included in the ordered list, or for odd length(**e**), one entry remains, in which case this entry is appended to the end of the list. The *K* elements chosen for refinement are then those corresponding to the last *K* entries in the list. The greedy refinement heuristic approached in this way can be evaluated in polynomial time. Note that the order in which we append e_i and e_j to the list for a given iteration will somewhat affect results. This effect becomes insignificant in practice once $K >> 1$. For the purpose of this paper, we place e_j before e_i. Figs. 6 and 7 show the results for the greedy refinement heuristic applied to *p*- and *h*-refinements, respectively.

We see from Figs. 6 and 7 that the adjoint-informed greedy refinement heuristic performs similarly to the magnitude refinement technique regarding error reduction over the range of tested *K* values. Comparing these figures to Figs. 4 and 5, note that, although both approaches trend downward rather smoothly [the improvement metric in (38) is strongly negative], this is not true of individual cases. By observation of the heuristic behavior for individual cases, we see there are several instances where the refinement of additional elements increases the error, sometimes substantially. Note, however, that very few cases exceed the initial $K = 0$ error for another *K*, i.e., the error may increase from one *K* to another, but rarely does it exceed the initial value ($K > 0$ still leads to a reduction in the initial error for almost all *K*). Exceptions to this, for instance in Fig. 6(d), tend to be for very narrow ranges of *K* making it less likely these undesirable *K*-values will be encountered by chance. This is reflected by a reduced occurrence and severity of these error-increasing *K* values for higher d*K*, for instance comparing Fig. 6(d) to Fig. 6(c).

This highlights and exemplifies the previously-stated desirability of heuristics that take into account aggregate cancellation effects—the tested heuristics perform better for higher d*K* as choosing a larger pool of refined elements increases the likelihood the error contribution of a given element will be sufficiently cancelled. Heuristics that group elements in one way or another are therefore often more effective. Note then, that the magnitude refinement heuristic applied to $dK > 1$ in this way now satisfies the previously stated desire for a heuristic taking into account aggregate effects.

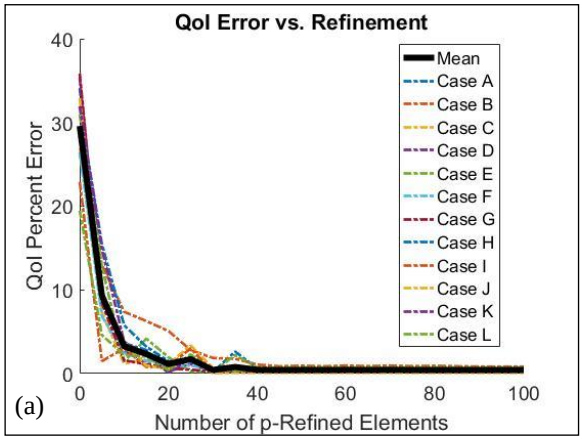

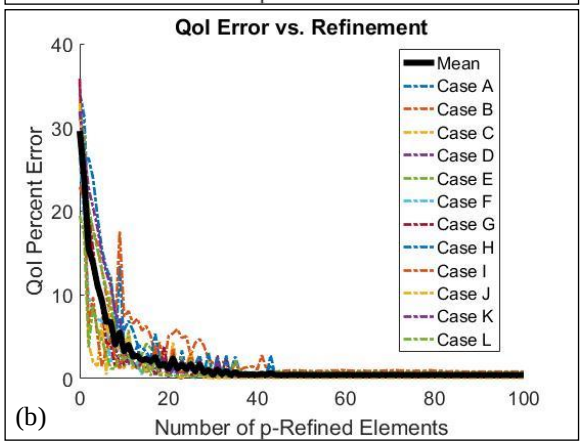

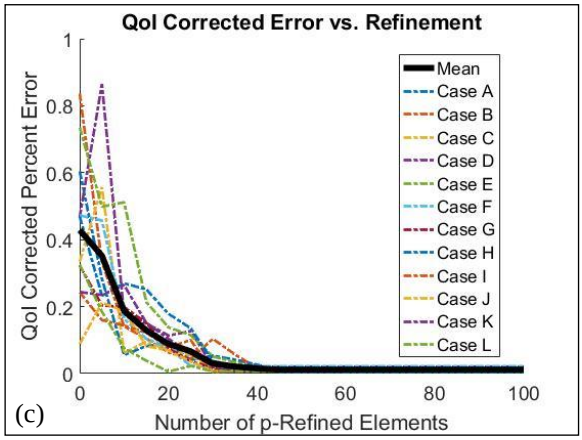

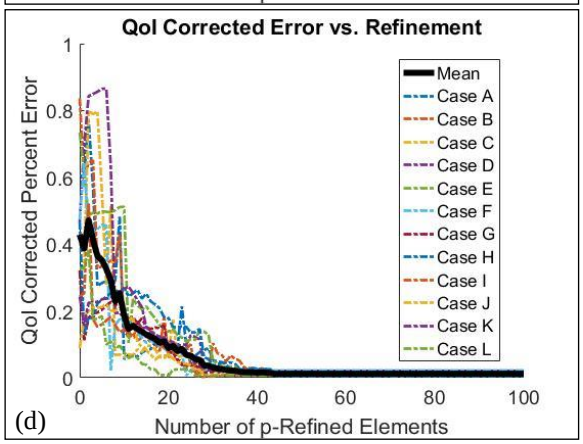

Fig. 6. The same as in Fig. 4 but for the greedy refinement method (implemented with *p*-refinement).

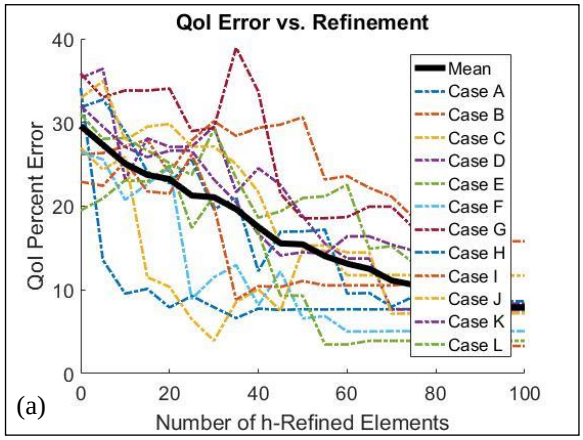

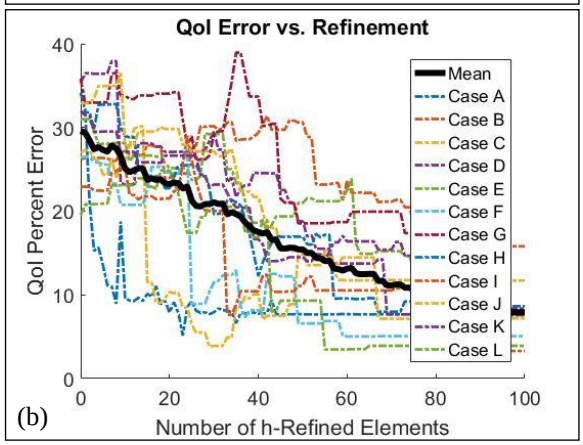

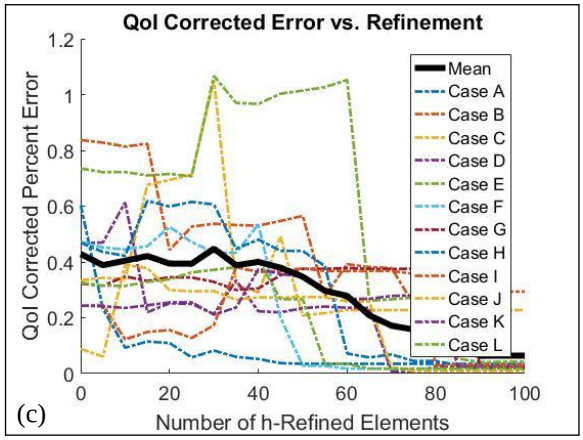

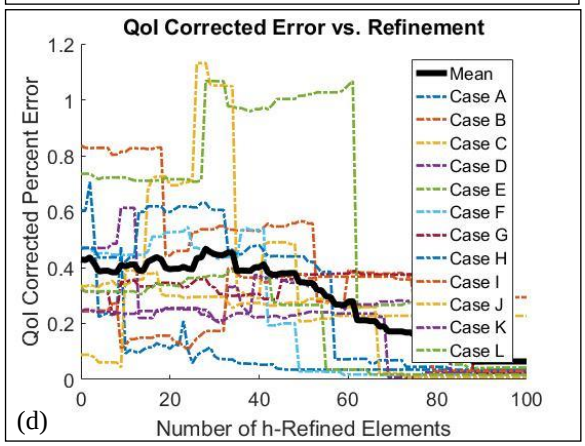

Fig. 7. The same as in Fig. 4 but for the greedy refinement method implemented with *h*-refinement.

The greedy refinement heuristic and magnitude refinement heuristic are evaluated against a benchmark refinement method in which K elements are chosen for refinement at random. Results for the random refinement heuristic are shown in Figs. 8 and 9 as applied to *p*- and *h*-refinements, respectively. Comparing these figures to the results for the two adjoint-informed heuristics, in Figs. 4–7, we see that, although the random refinement approach of course achieves the same error reduction for K = 100 (all elements refined), error reduction for nearly all other values of K is significantly worse.

Tables III and IV show improvement metric values, based on (38), for the results in Figs. 4–9 for *p*- and *h*-refinements, respectively. Examining the tables, we see that desirable vs. undesirable behavior of the heuristics demonstrated in Figs. 4–9 can be partially captured by the improvement metric, most notably their degree of monotonicity. Without exception, the metric is poorer (less negative) for applications of the heuristics with dK = 1 rather than dK = 5. This reflects the described grouping behavior advantageous to higher dK values. We also note that the random refinement heuristic presents lower metric values than the two adjoint-informed heuristics in all cases, indicating the superior performance of the adjoint-informed techniques. In addition, examining the results in Table IV in comparison to those in Table III, we note that, interestingly, although heuristics applied to *h*-refinement reduce error more slowly, they tend to do so somewhat more consistently, reflected in the higher improvement metric values for most entries in Table IV than the corresponding entries in Table III.

Table III: Improvement metric values based on (38) for magnitude, greedy, and random refinement heuristics applied toward *p*-refinement, i.e., for the results in Figs. 4, 6, and 8. The best value for each column has been bolded.

p-refinement	dK = 5		dK = 1	
Heuristic	Uncorrected	Corrected	Uncorrected	Corrected
Magnitude	**−0.3**	−0.2	**−0.22**	−0.20
Greedy	**−0.3**	**−0.4**	−0.08	**−0.28**
Random	−0.2	−0.3	−0.02	−0.0

Table IV: The same as in Table III but for *h*-refinement, i.e., for the results in Figs. 5, 7, and 9.

h-refinement	dK = 5		dK = 1	
Heuristic	Uncorrected	Corrected	Uncorrected	Corrected
Magnitude	−0.7	**−0.6**	**−0.38**	−0.10
Greedy	**−0.8**	−0.4	−0.22	**−0.12**
Random	−0.2	−0.0	−0.02	−0.04

V. Conclusions

This paper has investigated and evaluated useful applications of the adjoint problem and its solution for higher-order frequency-domain computational electromagnetics methods. Based on implementation of HOPS, QoI error estimation and error correction, element-wise error contribution estimate evaluation, and adjoint-informed automated targeted *p*- and *h*-refinements, this study has established and validated uses of adjoint techniques for improved efficiency, automation, and robustness of higher-order frequency-domain methods. Although the techniques applied in this paper have been demonstrated using a higher-order solver, all, with the exception of *p*-refinement, apply with no modification to low-order solvers. We have employed a one-dimensional higher-order PML-truncated FEM scattering solver as an ideal testbed for the ease of implementation, clarity of displaying the results, and intuitiveness of drawing conclusions from analyses, which then extend naturally to higher-dimensional solvers, more-complicated CEM techniques, adaptive CEM solutions, and problems requiring many solves.

Adjoint-based error estimation determines accurately whether a given discretization sufficiently describes a problem, and such error estimates can be applied to automated *h*- and *p*-refinement heuristics with little if any input from the user. Such heuristics reduce error quickly and vastly outperform a random refinement benchmark. On the tested problems, these heuristics are enough to reduce error by several orders of magnitude while only *p*-refining a modest number of elements (30/100) by one order using hierarchical basis functions and only four solves (two forward and two adjoint). Furthermore, these techniques can reduce error by a factor of more than 4.5 while *h*-refining roughly half of the elements in the domain (60/100). Most usefully, the adjoint-assisted *h*- and *p*-refinement methods we have demonstrated in this paper are near-monotonic in their error reduction with respect to number of refined elements. The usefulness of the demonstrated adjoint-informed refinement compounds with the *p*-refinement technique offered by higher-order FEM or MoM frequency-domain methods, especially on meshes already *h*-fine enough to describe the problem of interest, but nonetheless offers substantial error reduction and excellent convergence properties for low-order methods using *h*-refinement schemes. In fact, while heuristics applied to *h*-refinement reduce error more slowly, they result in higher improvement metric values than *p*-refinement.

To the best of our knowledge, this is the first demonstration of applicability of adjoint a posteriori error estimation techniques to adaptive discretization refinement in the field of CEM using arbitrary-order basis functions. In addition, among the novelties this work introduces to CEM are the application of a dual-weighted residual estimate to the adjoint-based a posteriori error estimation, the selective adaptivity based on error cancellation, and *p*-refinement using the adjoint solution. Unlike existing error estimates used in CEM that seek to bound error in a norm, the signed nature of this estimate is exploited to cancel local error contributions by grouping, leading to rapid reduction in global QoI error with a high selectivity. Our work has produced novel targeted model refinement heuristics that quickly and effectively reduce error in a quantity of interest. The study has demonstrated the exceptional benefits that adjoint techniques offer toward targeted, adaptive *h*- and *p*-refinement schemes using these heuristics. It has also attained a useful and broadly applicable improvement metric as a figure of merit for different refinement heuristics while providing an instructive discussion of the properties of a refinement heuristic that produce desirable values of this metric. In addition, we have demonstrated how HOPS can be used to obtain useful gradient information with respect to several parameters with vastly fewer additional solves than classical methods, requiring $n - 1$ fewer solves to compute the gradient, where n is the number

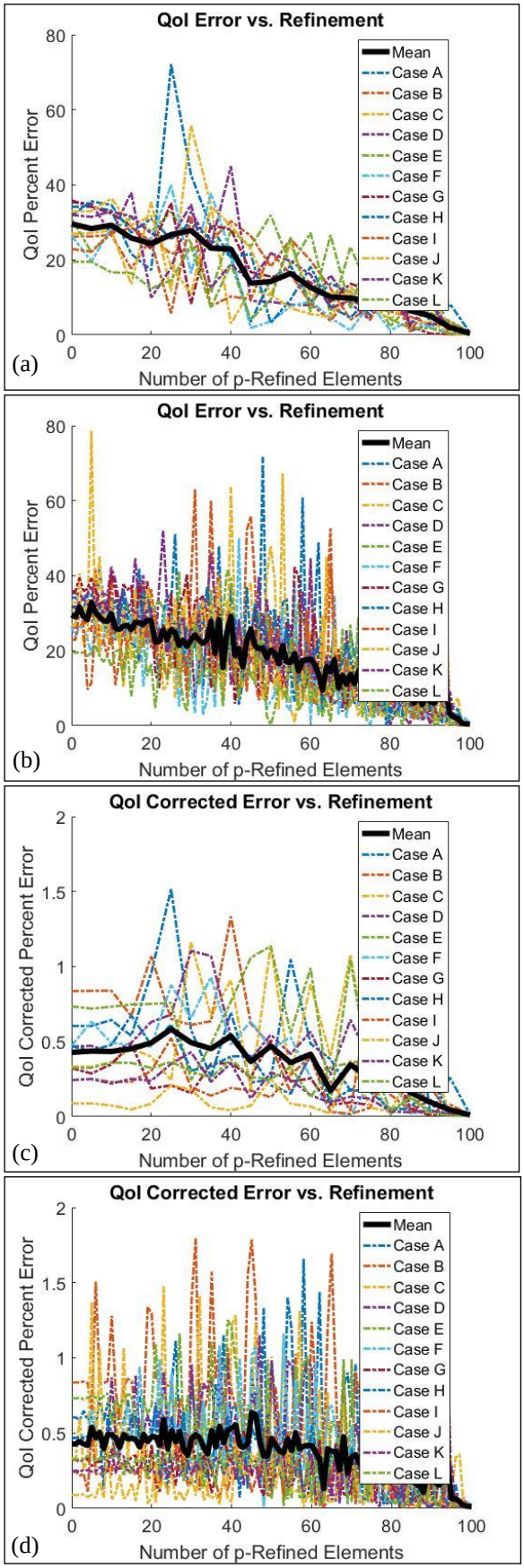

Fig. 8. The same as in Fig. 4 but for the random refinement method (implemented with *p*-refinement).

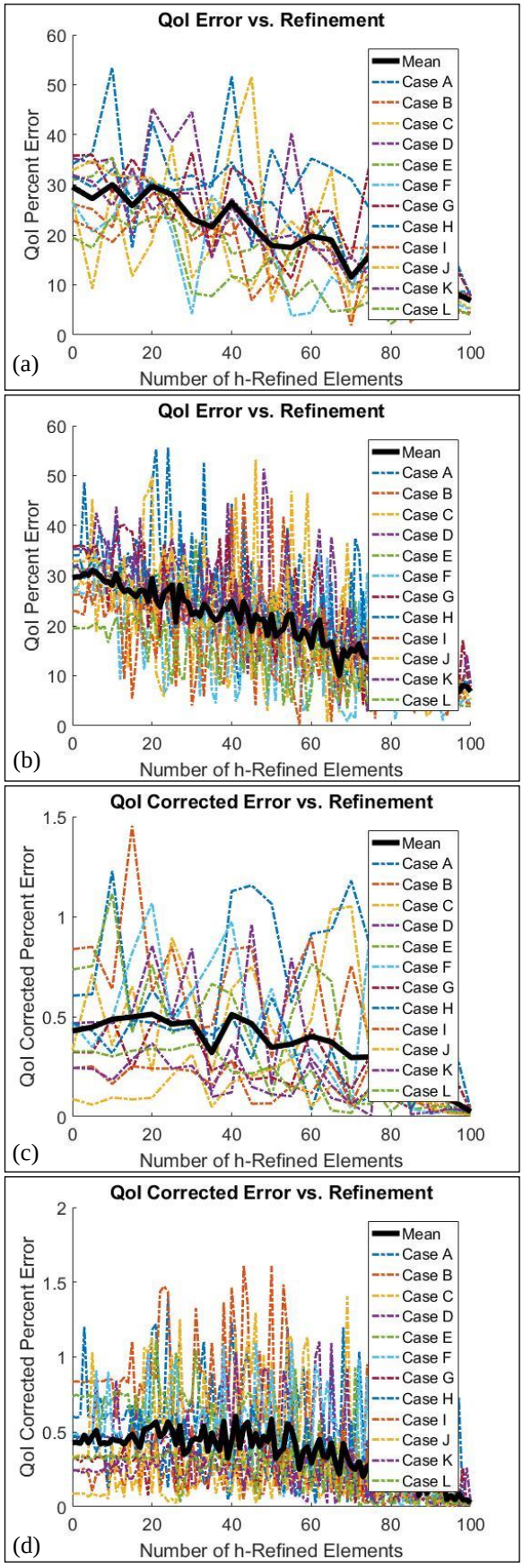

Fig. 9. The same as in Fig. 4 but for the random refinement method implemented with *h*-refinement.

of parameters with which the QoI varies. The additional applicability of this technique toward producing surrogate functions for optimization has also been shown. The surrogate functions generated, although piece-wise linear, closely match complicated QoI responses to various parameters.

In general, adjoint techniques are under-utilized in CEM where they could be applied to a wide variety of problems. The simple, one-dimensional FEM solver by which these relatively complicated adjoint techniques have been demonstrated for the purposes of this study should serve as a useful, easily replicable introduction to the described methods. The developed and evaluated adjoint techniques proposed and discussed in this paper may be used to derive and demonstrate useful applications of adjoint methods to more complicated CEM techniques and solvers. Namely, the methodology described in the paper generalizes well to higher dimensional problems by extension of, for instance, (11), (23), and (26) to the double-curl wave equation. In such a case, if three-dimensional problems are considered, the pertinent inner products become volume integrals of vector fields representing the three-dimensional measurement characteristic, forward field, and adjoint field. This study should be especially valuable for future development of adjoint-informed adaptive discretization *p*- and/or *h*-refinement schemes for such CEM techniques, as well as for adjoint-assisted CEM procedures applied to large-scale optimization problems, Monte Carlo simulations, RCS computation, and RF design problems among other uses.

ACKNOWLEDGEMENT

The authors would like to thank Dr. Michael Gilbert, Program Director, US Air Force Research Laboratory, CREATE SENTRi Program, for his support and guidance on the project and valuable discussions.

REFERENCES

[1] B. M. Notaroš, "Higher order frequency-domain computational electromagnetics," Special Issue on Large and Multiscale Computational Electromagnetics, *IEEE Transactions on Antennas and Propagation*, vol. 56, no. 8, pp. 2251-2276, August 2008.

[2] J. M. Jin, K. C. Donepudi, J. Liu, G. Kang, J. M. Song, and W. C. Chew, "High-Order Methods in Computational Electromagnetics," in *Fast and Efficient Algorithms in Computational Electromagnetics*, W. C. Chew *et al*, Ed. Norwood, MA: *Artech House*, 2001.

[3] B. M. Kolundzija and A. R. Djordjević, "Electromagnetic Modeling of Composite Metallic and Dielectric Structures", Norwood, MA: *Artech House*, 2002.

[4] A. F. Peterson, "Mapped Vector Basis Functions for Electromagnetic Integral Equations", *Morgan & Claypool Publishers*, 2006.

[5] R. D. Graglia, D. R. Wilton, and A. F. Peterson, "Higher order interpolatory vector bases for computational electromagnetics", *IEEE Transactions on Antennas and Propagation*, vol. 45, no. 3, pp. 329-342, March 1997.

[6] G. Kang, J. Song, W. C. Chew, K. C. Donepudi, and J. M. Jin, "A novel grid-robust higher order vector basis function for the method of moments," *IEEE Transactions on Antennas and Propagation*, vol. 49, pp. 908-915, June 2001.

[7] M. Djordjevic and B. M. Notaros, "Double higher order method of moments for surface integral equation modeling of metallic and dielectric antennas and scatterers," *IEEE Transactions on Antennas and Propagation*, vol. 52, no. 8, pp. 2118-2129, August 2004.

[8] E. Jørgensen, J. L. Volakis, P. Meincke, and O. Breinbjerg, "Higher order hierarchical Legendre basis functions for electromagnetic modeling," *IEEE Transactions on Antennas and Propagation*, vol. 52, pp. 2985-2995, November 2004.

[9] J. P. Webb, "Hierarchical vector basis functions of arbitrary order for triangular and tetrahedral finite elements", *IEEE Transactions on Antennas and Propagation*, vol. 47, no. 8, pp. 1244-1253, August 1999.G. Kron, *Diakoptics: The Piecewise Solution of Large Scale Systems*, MacDonald, 1963.

[10] M. M. Ilic and B. M. Notaros, "Higher order hierarchical curved hexahedral vector finite elements for electromagnetic modeling," *IEEE Transactions on Microwave Theory and Techniques*, vol. 51, no. 3, pp. 1026-1033, March 2003.

[11] M. M. Ilic and B. M. Notaros, "Higher order large-domain hierarchical FEM technique for electromagnetic modeling using Legendre basis functions on generalized hexahedra," *Electromagnetics*, vol. 26, no. 7, pp. 517-529, October 2006.

[12] M. M. Ilić, M. Djordjević, A. Ž. Ilić, and B. M. Notaroš, "Higher order hybrid FEM-MoM technique for analysis of antennas and scatterers," *IEEE Transactions on Antennas and Propagation*, vol. 57, pp. 1452-1460, May 2009.

[13] E. M. Klopf, N. J. Sekeljic, M. M. Ilić, and B. M. Notaroš, "Optimal Modeling Parameters for Higher Order MoM-SIE and FEM-MoM Electromagnetic Simulations," *IEEE Transactions on Antennas and Propagation*, *60*(6), 2790-2801, 2012

[14] D. E. Keyes, L. C. McInnes, C. Woodward, W. Gropp, E. Myra, M. Pernice, J. Bell, J. Brown, A. Clo, J. Connors, E. Constantinescu, D. Estep, K. Evans, C. Farhat, A. Hakim, G. Hammond, G. Hansen, J. Hill, T. Isaac, X. Jiao, K. Jordan, D. Kaushik, E. Kaxiras, A. Koniges, K. Lee, A. Lott, Q. Lu, J. Magerlein, R. Maxwell, M. McCourt, M. Mehl, R. Pawlowski, A. Peters Randles, D. Reynolds, B. Riviere, U. Ruede, T. Scheibe, J. Shadid, B. Sheehan, M. Shephard, A. Siegel, B. Smith, X. Tang, C. Wilson, and B. Wohlmuth, "Multiphysics simulations: Challenges and opportunities," *International Journal of High Performance Computing Applications*, vol. 27, no. 1, pp. 4-83, 2013.

[15] D. Estep. A posteriori error bounds and global error control for approximations of ordinary differential equations. *SIAM J. Numer. Anal.*, 32:1–48, 1995.

[16] K. Eriksson, D. Estep, P. Hansbo, and C. Johnson. Introduction to adaptive methods for differential equations. *Acta Numerica*, pages 105–158, 1995.

[17] K. Eriksson, D. Estep, P. Hansbo, and C. Johnson. *Computational Differential Equations*. Cambridge University Press, New York, 1996.

[18] M. Giles and E. Suli, "Adjoint methods for PDEs: A posteriori error analysis and postprocessing by duality," *Acta Numerica*, pp. 145-236, 2002.

[19] R. Becker and R. Rannacher, "An optimal control approach to a posteriori error estimation in finite element methods," *Acta Numerica*, pp. 1-102, 2001.

[20] W. Bangerth and R. Rannacher. *Adaptive Finite Element Methods for Differential Equations* Birkhauser, Boston, 2003.

[21] M. H. Bakr, *Nonlinear Optimization in Electrical Engineering with Applications in MATLAB*, IET, September 2013.

[22] M. H. Bakr and N. K. Nikolova, "An adjoint variable method for time domain TLM with fixed structured grids," *IEEE Transactions on Microwave Theory and Techniques*, vol. 52, pp 554-559, 2004.

[23] N. K. Nikolova, H. W. Tam, and M. H. Bakr, "Sensitivity analysis with the FDTD method on structures grids," *IEEE Transactions on Microwave Theory and Techniques*, vol. 52, no2, pp. 1207-1216, 2004.

[24] S. M. Ali, N. K. Nikolova, and M. H. Bakr, "A central adjoint variable method for sensitivity analysis," *IEEE Transactions on Magnetics*, vol. 40, no. 4, pp. 1969-1971, 2004.

[25] M. A. Swillam, M. H. Bakr, and X. Li, "Accurate sensitivity analysis of photon devices exploiting the finite-difference time-domain central adjoint variable method," *Journal of Applied Optics*, vol. 46, no. 9, pp. 1492-1499, 2007.

[26] M. A. Swillam, M. H. Bakr, N. K. Nikolova, and X. Li, "Adjoint sensitivity analysis of dielectric discontinuities using FDTD," *Journal of Electromagnetics*, vol. 27, no. 2, pp 123-140, 2007.

[27] M. H. Bakr and N. K. Nikolova, "An adjoint variable method for time-domain transmission-line modeling with fixed structured grids," *IEEE Transactions on Microwave Theory and Techniques*, vol. 52, no. 2, pp. 449-554, 2004.

[28] P. Garcia, and J. P. Webb, "Optimization of planar devices by the finite element method," *IEEE Transactions on Microwave Theory and Techniques*, vol. 38, pp. 48-53, 1990.

[29] S. Koziel and A. Bekasiewicz, "Fast EM-driven size reduction of antenna structures by means of adjoint sensitivities and trust regions,"

IEEE Antennas and Wireless Propagation Letters, vol. 14, pp. 1681-1684, 2015.

[30] M. M. Botha and D. B. Davidson, "An explicit a posteriori error indicator for electromagnetic, finite element-boundary integral analysis," in *IEEE Transactions on Antennas and Propagation*, vol. 53, no. 11, pp. 3717-3725, Nov. 2005.

[31] K. C. Chellamuthu and N. Ida, "'A posteriori' element by element local error estimation technique and 2D & 3D adaptive finite element mesh refinement," *IEEE Transactions on Magnetics*, vol. 30, no. 5, pp. 3527-3530, Sept. 1994.

[32] S. M. Schnepp, "Error-driven dynamical hp-meshes with the Discontinuous Galerkin Method for three-dimensional wave propagation problems," *Journal of Computational and Applied Mathematics*, vol. 270, pp. 353-368, 2014.

[33] F. C Meyer and D. B. Davidson, "A posteriori error estimates for two-dimensional electromagnetic field computations: boundary elements and finite elements," *ACES Journal*, vol. 11, no. 2, pp. 40-54, 1996.

[34] K. C. Chellamuthu and N. Ida, "Reliability assessment of an 'a posteriori' error estimate for adaptive computation of electromagnetic field problems," in *IEEE Transactions on Magnetics*, vol. 31, no. 3, pp. 1761-1764, May 1995.

[35] P. Monk, "A posteriori error indicators for Maxwell's equations," *Journal of Computational and Applied Mathematics*, vol. 100, no. 2, pp. 173-190, Dec. 1998.

[36] P. Monk and E. Suli, "The adaptive computation of far-field patterns by a posteriori error estimation of linear functionals," *SIAM Journal of Numerical Analysis*, vol. 36 no. 1, pp. 251-274, 1998.

[37] D. Estep and D. Neckels, "Fast and Reliable Methods for Determining the Evolution of Uncertain Parameters in Differential Equations," *J. Comp. Physics*, vol. 213, pp. 530-556, April 2006.

[38] G. I. Marchuk, Adjoint Equations and Analysis of Complex Systems, Netherlands: Kluwer Academic Publishers; 1995.

[39] C. Key, A. Smull, B. M. Notaroš, D. Estep, and T. Butler, "Adjoint Methods for Uncertainty Quantification in Applied Computational Electromagnetics: FEM Scattering Examples," *Proceedings of the 2018 International Applied Computational Electromagnetics Society Symposium – ACES2018*, March 25–29, 2018, Denver, Colorado, USA.

[40] C. Key, A. Smull, D. Estep, T. Butler, and B. M. Notaroš, "A Posteriori Element-wise Error Quantification for FEM Solvers Using Higher Order Basis Functions," *Proceedings of the 2018 IEEE International Symposium on Antennas and Propagation*, July 8–13, 2018, Boston, MA, USA, pp. 1319–1320.

[41] B. M. Notaroš, Electromagnetics, New Jersey : PEARSON Prentice Hall; 2010.

[42] A. B. Manić, S. B. Manić, M. M. Ilić, and B. M. Notaroš, "Large anisotropic inhomogeneous higher order hierarchical generalized hexahedral finite elements for 3-D electromagnetic modeling of scattering and waveguide structures," *Microw. Opt. Technol. Lett.*, vol. 54, pp. 1644–1649, Jul. 2012.

[43] A. P. Smull, A.B. Manic, S.B. Manic, and B.M. Notaros, "Anisotropic Locally Conformal Perfectly Matched Layer for Higher Order Cuvilinear Finite Element Modeling," IEEE Transactions on Antennas and Propagation, vol. 65, no. 12, pp. 7157-7165, December 2017.

[44] D. Estep, M. Larson, and R. Williams, "Estimating the error of numerical solutions of systems of nonlinear reaction-diffusion equations," *Memoirs of the American Mathematical Society*, vol. 696, pp. 1-109, 2000.

[45] J. H. Chaudhry, D. Estep, S. Tavener, V. Carey, and J. Sandelin, "A Posteriori Error Analysis of Two-Stage Computation Methods with Application to Efficient Discretization and the Parareal Algorithm," *SIAM Journal on Numerical Analysis*, vol. 54, pp. 2729-3122, 2016.

Cam Key (S'16) was born in Fort Collins, CO in 1996. He received his B.S. (2018) and is currently pursuing his Ph.D. in Electrical and Computer Engineering from Colorado State University. His current research interests include uncertainty quantification, error prediction, and optimization for computational science and engineering; computational geometry, meshing, data science, machine learning, artificial intelligence, remote sensing and GIS, and novel applications of numerical methods across disciplines.

Aaron P. Smull (S'15) was born in Santa Rosa, California in 1993. He received his B.S. (2015) and M.S. (2017) in Electrical Engineering from Colorado State University, and is currently pursuing his PhD in physics and the University of California, Berkeley. His current research interests include the development of numerical algorithms for the classical and quantum interaction of electromagnetic waves with matter, and the development of novel quantum information processing technologies.

Donald Estep received his B.A. in Mathematics from Columbia University in 1981 and his M.S. and Ph.D. in Applied Mathematics from the University of Michigan in 1987.

From 1987-2002, he was a faculty member in the School of Mathematics at the Georgia Institute of Technology. He joined the Department of Mathematics at Colorado State University in 2000 and moved to the Department of Statistics in 2006, serving as Chair from 2017-2019. In 2019, he moved to the Department of Statistics and Actuarial Science at Simon Fraser University to assume the position of Director of the Canadian Statistical Sciences Institute.

Dr. Estep was appointed University Interdisciplinary Research Scholar in 2009 and University Distinguished Professor in 2017 at Colorado State University. He served as Co-Organizer and first Chair of the SIAM Activity Group on Uncertainty Quantification from 2010-12, and Co-Editor in Chief (founding) of the SIAM/ASA Journal on Uncertainty Quantification from 2012-2017. He won the Computational and Mathematical Methods in Science and Engineering Prize in 2005, held the Chalmers Jubilee Professorship at Chalmers University of Technology from 2013-2014, and was appointed Fellow of the Society for Industrial and Applied Mathematics in 2014.

Troy Butler received his B.S. in electrical engineering (2003) followed by his M.S. (2005) and Ph.D. (2009) in mathematics from Colorado State University.

From 2009-12, Dr. Butler was a Postdoctoral Research Fellow (2009-11) and Research Associate (2011-12) in the Computational Hydraulics Group housed within the Institute for Computational Engineering and Sciences at The University of Texas at Austin. From 2012-13, Dr. Butler was a Research Scientist in the Department of Statistics at Colorado State University. In Fall 2013, Dr. Butler joined CU Denver as an Assistant Professor in Mathematical and Statistical Sciences and was promoted with tenure to Associate Professor in 2019. From 2014-17, Dr. Butler served as the Director for the Center for Computational Mathematics at CU Denver.

Branislav M. Notaroš (M'00-SM'03-F'16) received the Dipl.Ing. (B.S.), M.S., and Ph.D. degrees in electrical engineering from the University of Belgrade, Belgrade, Yugoslavia, in 1988, 1992, and 1995, respectively.

From 1996 to 1999, he was Assistant Professor in the School of Electrical Engineering at the University of Belgrade. He was Assistant and Associate Professor from 1999 to 2006 in the Department of Electrical and Computer Engineering at the University of Massachusetts Dartmouth. He is currently Professor of Electrical and Computer Engineering, University Distinguished Teaching Scholar, and Director of Electromagnetics Laboratory at Colorado State University.

Dr. Notaroš serves as General Chair of the 2022 IEEE International Symposium on Antennas and Propagation and USNC-URSI National Radio Science Meeting and is Associate Editor for the IEEE Transactions on Antennas and Propagation. He serves as Vice President of Applied Computational Electromagnetics Society (ACES) and as Vice-Chair of USNC-URSI Commission B. He was the recipient of the 2005 IEEE MTT-S Microwave Prize, 1999 IEE Marconi Premium, 2019 ACES Technical Achievement Award, 2015 ASEE ECE Distinguished Educator Award, 2015 IEEE Undergraduate Teaching Award, and many other research and teaching international and national awards.